Heliyon 8 (2022) e09612

Contents lists available at ScienceDirect

Heliyon

journal homepage: www.cell.com/heliyon

Research article

Production of $(Sm,Zr)(Fe,Co)_3$ magnets

Tetsuji Saito *

Department of Advanced Materials Science and Engineering, Chiba Institute of Technology, Narashino, Chiba 275-8588, Japan

ARTICLE INFO

Keywords:
Sm-Fe alloys
Melt spinning
Coercivity

ABSTRACT

This study was aimed at the improvement of $SmFe_3$-based alloys prepared by means of melt-spinning. A systematic study was carried out on $(Sm_{1-x}Zr_x)(Fe_{0.75}Co_{0.25})_3$ (x = 0–0.4) alloys melt-spun at a wheel speed of 50 m/s and annealed at 773–1173 K. $SmFe_3$-based melt-spun ribbons with a rhombohedral structure were prepared from the $(Sm_{1-x}Zr_x)$ $(Fe_{0.75}Co_{0.25})_3$ (x = 0–0.4) alloys. The addition of zirconium increased the coercivity and enhanced the remanence of the melt-spun ribbons. However, the Curie temperature slightly decreased with increasing zirconium content. The optimally annealed alloys, with a composition of $(Sm_{0.7}Zr_{0.3})$ $(Fe_{0.75}Co_{0.25})_3$, achieved a coercivity of 7.8 kOe, a remanence of 6.0 kG, and a Curie temperature of 680K.

1. Introduction

Accompanying the realization of high-performance Nd-Fe-B permanent magnets, R&D of new permanent magnets has been largely concentrated on rare-earth-based alloys [1, 2, 3, 4, 5]. Nd-Fe-B permanent magnets are utilized in a broad variety of advanced electromagnetic devices, including motors for hybrid and electric vehicles. Due to the tremendous increase in the industrial production of Nd-Fe-B permanent magnets, the supply of rare-earth elements is an issue that is currently a focus of concern [6, 7, 8]. The rare-earth elements are not particularly uncommon, and in fact some rare-earth elements are found in greater abundance than many widely used elements such as lead. The problem with regard to the rare-earth elements is the balance between the supply and demand [9, 10, 11]. As a result, some rare-earth elements are produced in larger amounts than required, and these resources are simply stockpiled. Therefore, increasing demand for the Nd metal has motivated intensified research on the rare-earth-lean magnets and rare-earth magnets without Nd.

One of the candidates for new permanent magnet materials is the $Sm_2Fe_{17}N_3$ magnet, which has been produced by nitrogenation of the Sm_2Fe_{17} phase [12, 13, 14, 15]. $Sm_2Fe_{17}N_3$ magnets have not been obtained by sintering, however, because the $Sm_2Fe_{17}N_3$ phase decomposes during the high-temperature sintering process [16]. Thus, studies on $Sm_2Fe_{17}N_3$ sintered magnets are still underway [17, 18, 19]. As an alternative to $Sm_2Fe_{17}N_3$ magnets, other Sm-based intermetallic compounds of the $SmFe_3$ phase have also been studied. The $SmFe_3$ phase has a rhombohedral $PuNi_3$-type structure and possesses a large anisotropy field [20, 21]. In order to realize $SmFe_3$-based magnets, it is essential to improve the magnetic properties of the $SmFe_3$ phase [22, 23, 24]. It was found that the $(Sm,Zr)Fe_3$ magnets exhibited a high coercivity [24]. However, the reported remanence of the $(Sm,Zr)Fe_3$ magnets is not yet satisfactory. Since it is known that the substitution of Co for Fe in the Sm_2Fe_{17} phase results in enhanced magnetization [25, 26, 27], the effects of Zr substitution on the structure and magnetic properties of melt-spun and annealed alloys with an $(Sm_{1-x}Zr_x)$ $(Fe_{0.75}Co_{0.25})_3$ (x = 0–0.4) composition were investigated. The changes in the magnetic properties of the $SmFe_3$-based magnets as a consequence of annealing were systematically monitored.

2. Experimental

$(Sm_{1-x}Zr_x)(Fe_{0.75}Co_{0.25})_3$ (x = 0–0.4) alloy ingots were prepared by induction melting and the starting alloy contained 15% excess of Sm compared with the normal stoichiometry to compensate for losses of Sm such as by oxidation and vaporization during melting and melt-spinning. Melt-spun ribbons of $(Sm_{1-x}Zr_x)(Fe_{0.75}Co_{0.25})_3$ (x = 0–0.4) alloys were obtained by melt-spinning using a copper wheel (Vs = 50 m/s) in an argon atmosphere. Annealing of the as-quenched melt-spun ribbons was performed in an argon atmosphere for 1 h at different temperatures in the range of 773–1173 K. The structures and magnetic properties of $(Sm,Zr)(Fe,Co)_3$ melt-spun ribbons were investigated in the as-quenched condition and after annealing. The crystallographic structure was determined by X-ray diffraction (XRD) using a MiniFlex600 X-ray diffractometer (Rigaku) and by differential thermal analysis (DTA) using an STA 7300 thermal analysis system (Hitachi). The magnetic properties were investigated using a BHV-525RSCM vibrating sample magnetometer

* Corresponding author.
E-mail address: tetsuji.saito@it-chiba.ac.jp.

https://doi.org/10.1016/j.heliyon.2022.e09612
Received 31 January 2022; Received in revised form 27 March 2022; Accepted 27 May 2022

(VSM) (Riken Denshi). The thermomagnetic analysis (TMA) curves of the specimens were measured in a small magnetic field of 0.5 kOe using the VSM. The slope of the thermomagnetic curve near the Curie temperature was determined by curve fitting and the Curie temperature was determined by extrapolation. The hysteresis loops of the specimens were measured with a maximum applied magnetic field of 25 kOe using the VSM after the specimens had been pulverized and embedded in paraffin.

3. Results and discussion

The XRD patterns of the as-quenched $(Sm_{1-x}Zr_x)(Fe_{0.75}Co_{0.25})_3$ (x = 0–0.4) melt-spun ribbons are shown in Figure 1. Only a broad halo peak is seen in the XRD patterns of the $(Sm_{1-x}Zr_x)(Fe_{0.75}Co_{0.25})_3$ (x = 0–0.2) specimens. This indicates that the as-quenched $Sm(Fe_{0.75}Co_{0.25})_3$ specimen was amorphous and that a small amount of Zr substitution did not alter the amorphous phase. In contrast, small and somewhat broad diffraction peaks of the $SmFe_3$ phase are noted in the XRD patterns of the $(Sm_{1-x}Zr_x)(Fe_{0.75}Co_{0.25})_3$ (x = 0.3–0.4) specimens. This suggests that a larger amount of Zr substitution led to the formation of the crystalline $SmFe_3$ phase.

In order to investigate the crystallization behavior of the specimens, the DTA curves of the as-quenched $(Sm_{1-x}Zr_x)(Fe_{0.75}Co_{0.25})_3$ (x = 0–0.4) melt-spun ribbons were measured (Figure 2). The DTA curves of the $(Sm_{1-x}Zr_x)(Fe_{0.75}Co_{0.25})_3$ (x = 0–0.3) specimens have an exothermic peak, which corresponds to the crystallization from the amorphous phase. The exothermic peaks shift to a higher temperature from 850 K for the $Sm(Fe_{0.75}Co_{0.25})_3$ specimen to 880 K for the $(Sm_{0.7}Zr_{0.3})(Fe_{0.75}Co_{0.25})_3$ specimen with increasing Zr content. This suggests that these specimens consisted of the amorphous phase and that the thermal stability of the amorphous phase increased with increasing Zr content. However, no exothermic peak was seen in the DTA curve of the $(Sm_{0.6}Zr_{0.4})(Fe_{0.75}Co_{0.25})_3$ specimen, confirming that the specimen did not contain any amorphous phase. These results indicate that whether the amorphous phase was obtained or not was dependent on the Zr content of the specimens. In the as-quenched state, the $(Sm_{1-x}Zr_x)(Fe_{0.75}Co_{0.25})_3$ (x = 0–0.2) specimens were amorphous, but the $(Sm_{0.7}Zr_{0.3})(Fe_{0.75}Co_{0.25})_3$ specimen consisted of the amorphous and $SmFe_3$ phases and the $(Sm_{0.6}Zr_{0.4})(Fe_{0.75}Co_{0.25})_3$ specimen was composed of the $SmFe_3$ phase.

Figure 3 shows the hysteresis loops of the as-quenched $(Sm_{1-x}Zr_x)(Fe_{0.75}Co_{0.25})_3$ (x = 0–0.4) melt-spun ribbons. Narrow hysteresis loops were obtained from the $(Sm_{1-x}Zr_x)(Fe_{0.75}Co_{0.25})_3$ (x = 0–0.2) specimens. The hysteresis loop of the $(Sm_{0.7}Zr_{0.3})(Fe_{0.75}Co_{0.25})_3$ specimen (red lines) was wider than that of the $(Sm_{1-x}Zr_x)(Fe_{0.75}Co_{0.25})_3$ (x = 0–0.2) specimens but was not smooth. Such a constrained hysteresis loop is usually observed in the specimen consisting of two magnetic phases with different coercivity [28]. This is consistent with the results of the XRD and DTA studies, indicating that the $(Sm_{0.7}Zr_{0.3})(Fe_{0.75}Co_{0.25})_3$ specimen consisted of the amorphous and $SmFe_3$ phases. The widest hysteresis loop (purple lines) was obtained from the $(Sm_{0.6}Zr_{0.4})(Fe_{0.75}Co_{0.25})_3$ specimen,

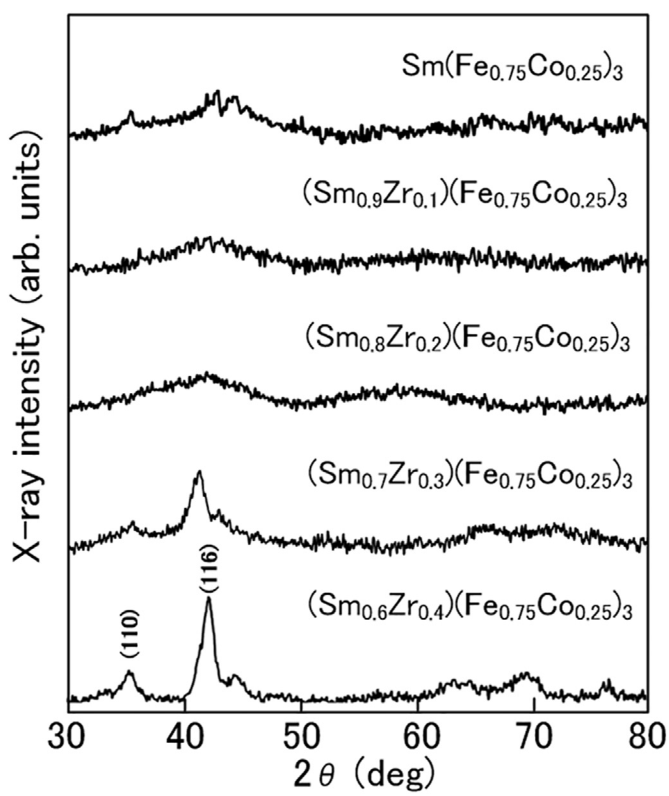

Figure 1. XRD patterns of as-quenched $(Sm_{1-x}Zr_x)(Fe_{0.75}Co_{0.25})_3$ (x = 0–0.4) melt-spun ribbons.

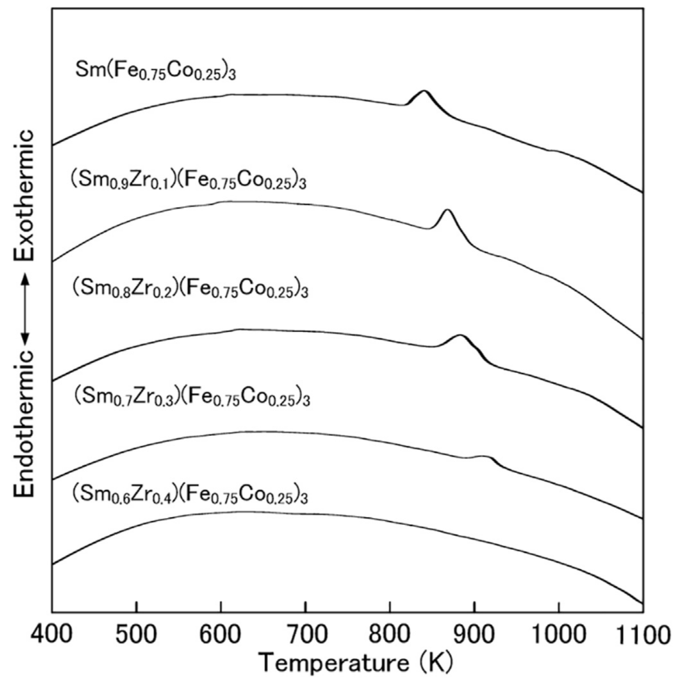

Figure 2. DTA curves of as-quenched $(Sm_{1-x}Zr_x)(Fe_{0.75}Co_{0.25})_3$ (x = 0–0.4) melt-spun ribbons.

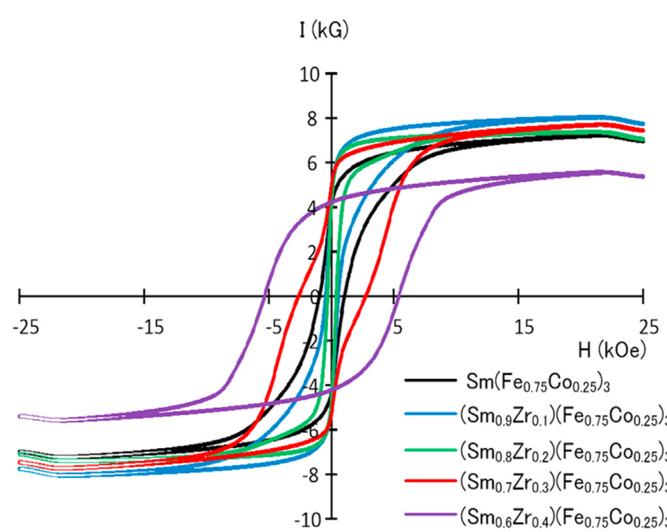

Figure 3. Hysteresis loops of as-quenched $(Sm_{1-x}Zr_x)(Fe_{0.75}Co_{0.25})_3$ (x = 0–0.4) melt-spun ribbons.

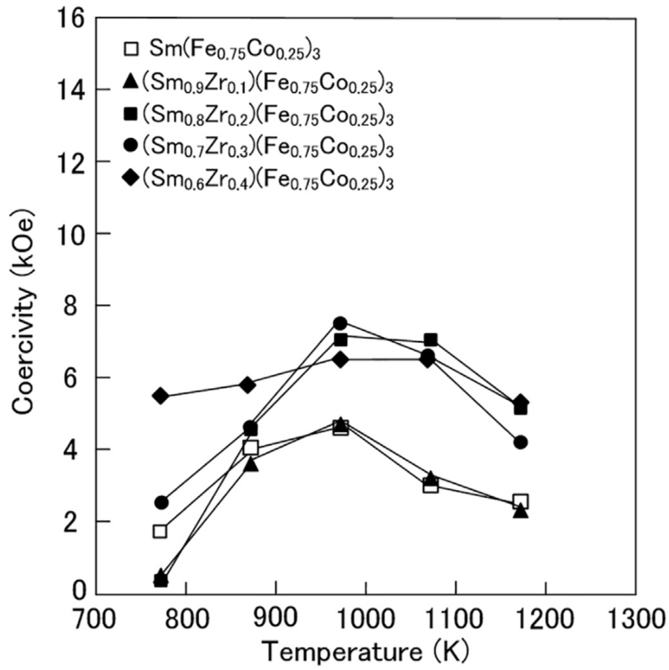

Figure 4. Coercivity of $(Sm_{1-x}Zr_x)(Fe_{0.75}Co_{0.25})_3$ (x = 0–0.4) melt-spun ribbons as a function of the annealing temperature.

which was composed of the $SmFe_3$ phase. Thus, the observed coercivity of 5.2 kOe in the $(Sm_{0.6}Zr_{0.4})(Fe_{0.75}Co_{0.25})_3$ specimen is believed to be attributed to the existence of the $SmFe_3$ phase.

The change in the magnetic properties of the melt-spun ribbons due to crystallization from the amorphous phase to the $SmFe_3$ phase was investigated. Figure 4 shows the coercivity of the $(Sm_{1-x}Zr_x)(Fe_{0.75}Co_{0.25})_3$ (x = 0–0.4) melt-spun ribbons as a function of the annealing temperature. The $(Sm_{1-x}Zr_x)(Fe_{0.75}Co_{0.25})_3$ (x = 0–0.3) specimens with the amorphous phase exhibited a large increase in coercivity when annealed at 873 K or higher. This is due to the crystallization of the $SmFe_3$ phase. A slight increase in coercivity was noted in the $(Sm_{0.6}Zr_{0.4})(Fe_{0.75}Co_{0.25})_3$ specimen, which contained the $SmFe_3$ phase but not the amorphous phase. The coercivity reached the maximum value at an annealing temperature of 973 K regardless of the Zr content. Thus, 973 K was determined to be the optimal annealing temperature of the $(Sm_{1-x}Zr_x)(Fe_{0.75}Co_{0.25})_3$ (x = 0–0.4) melt-spun ribbons. The highest coercivity of 7.8 kOe was recorded in the optimally annealed $(Sm_{0.7}Zr_{0.3})(Fe_{0.75}Co_{0.25})_3$ specimen.

The optimally annealed $(Sm_{1-x}Zr_x)(Fe_{0.75}Co_{0.25})_3$ (x = 0–0.4) melt-spun ribbons consisted of the $SmFe_3$ phase, as shown by their XRD patterns in Figure 5. The magnetic properties of the optimally annealed melt-spun ribbons were then examined. Figure 6 shows the hysteresis loops of the optimally annealed $(Sm_{1-x}Zr_x)(Fe_{0.75}Co_{0.25})_3$ (x = 0–0.4) melt-spun ribbons. The corresponding TMA curves are shown in Figure 7. Although the hysteresis loops of the $(Sm_{1-x}Zr_x)(Fe_{0.75}Co_{0.25})_3$ (x = 0–0.2) specimens became

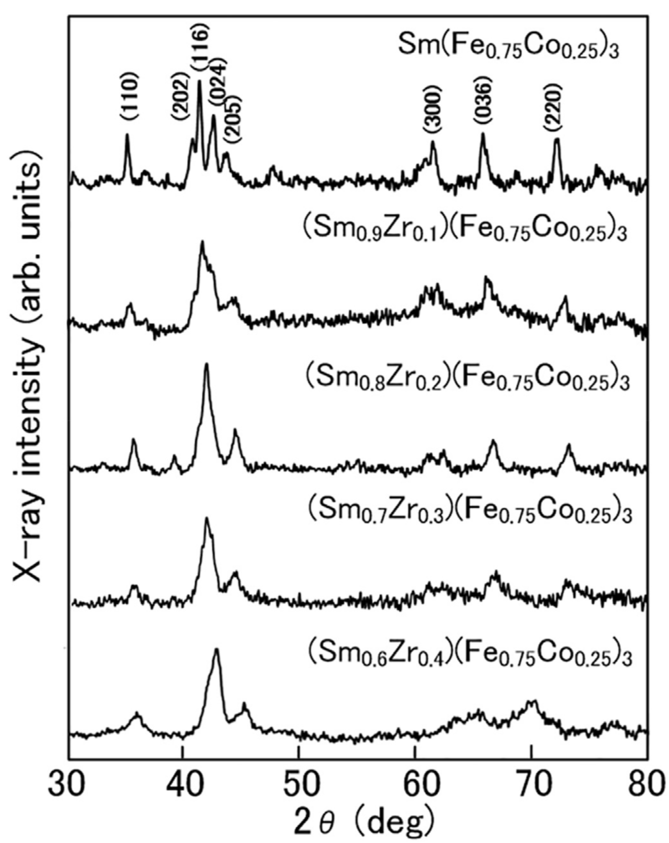

Figure 5. XRD patterns of optimally annealed $(Sm_{1-x}Zr_x)(Fe_{0.75}Co_{0.25})_3$ (x = 0–0.4) melt-spun ribbons.

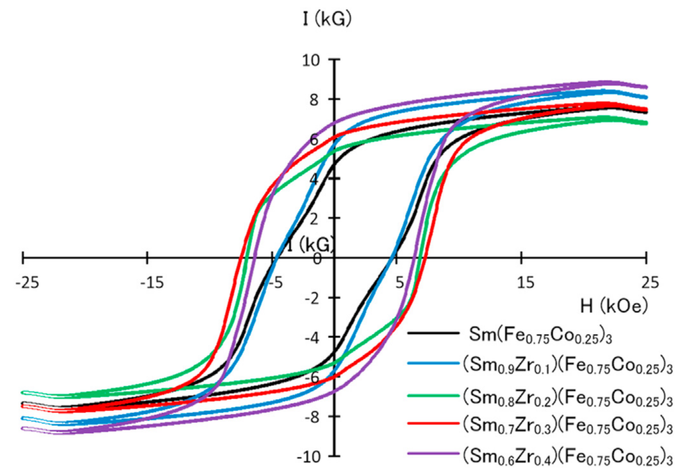

Figure 6. Hysteresis loops of optimally annealed $(Sm_{1-x}Zr_x)(Fe_{0.75}Co_{0.25})_3$ (x = 0–0.4) melt-spun ribbons.

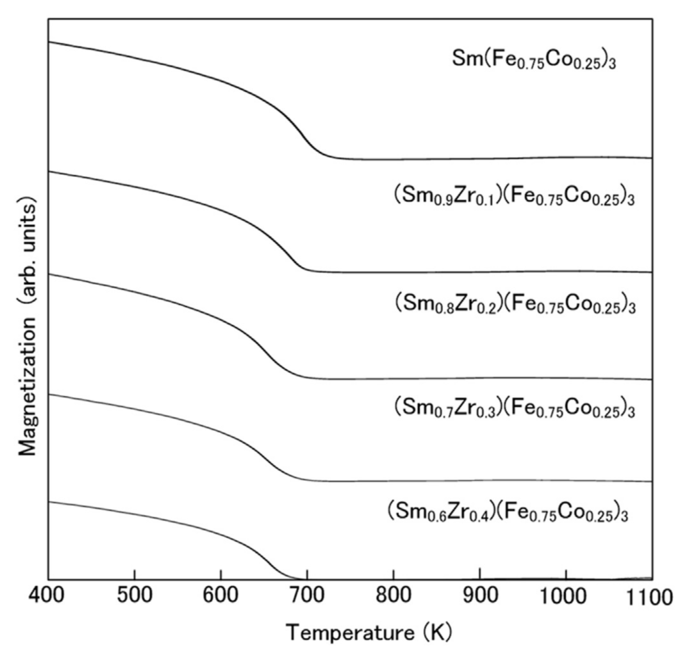

Figure 7. TMA curves of optimally annealed $(Sm_{1-x}Zr_x)(Fe_{0.75}Co_{0.25})_3$ (x = 0–0.4) melt-spun ribbons.

wider than those of the as-quenched specimens, the loops were not smooth but contained kinks. The constrained hysteresis loops imply that these specimens consisted of two magnetic phases with different coercivity. However, the TMA curves of the $(Sm_{1-x}Zr_x)(Fe_{0.75}Co_{0.25})_3$ (x = 0–0.2) specimens showed only one magnetic transition at 720 K, indicating that the specimens consisted of one magnetic phase. Therefore, the origin of the constrained hysteresis loops is considered to be different grain sizes in the $SmFe_3$ phases, which exhibited different coercivity. A further microstructural study is necessary to confirm this. On the other hand, the $(Sm_{1-x}Zr_x)(Fe_{0.75}Co_{0.25})_3$ (x = 0.3–0.4) specimens exhibited smooth hysteresis loops. The TMA curves also showed only one magnetic transition, which corresponded to the Curie temperature. It is noted that the Curie temperature of the $(Sm_{1-x}Zr_x)(Fe_{0.75}Co_{0.25})_3$ (x = 0–0.4) specimens became lower with increasing the Zr content. The $(Sm_{0.7}Zr_{0.3})(Fe_{0.75}Co_{0.25})_3$ specimen showed the highest coercivity of 7.8 kOe with a remanence of 6.0 kG and a Curie temperature of 680 K, while the $(Sm_{06}Zr_{0.4})(Fe_{0.75}Co_{0.25})_3$ specimen exhibited the highest remanence of 7.0 kG with a coercivity of 7.0 kOe and a Curie temperature of 670 K.

4. Conclusion

(1) As-quenched melt-spun ribbons of $(Sm_{1-x}Zr_x)(Fe_{0.75}Co_{0.25})_3$ (x = 0–0.2) alloys were found to be amorphous and showed low coercivity, while those of $(Sm_{1-x}Zr_x)(Fe_{0.75}Co_{0.25})_3$ (x = 0.3–0.4) alloys consisted of either the $SmFe_3$ and amorphous phases or the $SmFe_3$ phase and exhibited a higher coercivity.
(2) The optimal annealing temperature of the $(Sm_{1-x}Zr_x)(Fe_{0.75}Co_{0.25})_3$ (x = 0–0.2) alloys was 973 K. The optimally annealed specimens consisted of the $SmFe_3$ phase. The TMA studies revealed that the Curie temperature of the optimally annealed specimens decreased, from 720 K for the $Sm(Fe_{0.75}Co_{0.25})_3$ specimen to 670 K for the $(Sm_{06}Zr_{0.4})(Fe_{0.75}Co_{0.25})_3$ specimen, as the Zr content increased.
(3) The highest coercivity of 7.8 kOe was achieved in the optimally annealed $(Sm_{0.7}Zr_{0.3})(Fe_{0.75}Co_{0.25})_3$ specimen, while the highest remanence of 7.0 kG was obtained in the optimally annealed $(Sm_{0.6}Zr_{0.4})(Fe_{0.75}Co_{0.25})_3$ specimen.

Declarations

Author contribution statement

Tetsuji Saito: Conceived and designed the experiments; Performed the experiments; Analyzed and interpreted the data; Contributed reagents, materials, analysis tools or data; Wrote the paper.

Funding statement

This research did not receive any specific grant from funding agencies in the public, commercial, or not-for-profit sectors.

Data availability statement

Data will be made available on request.

Declaration of interest's statement

The authors declare no conflict of interest.

Additional information

No additional information is available for this paper.

References

[1] S. Hirosawa, Current status of research and development toward permanent magnets free from critical elements, J. Magn. Soc. Jpn. 39 (2015) 85–95.
[2] A. Trench, J.P. Sykes, Rare Earth Permanent Magnets and Their Place in the Future Economy, Engineering 6 (2020) 115–117.
[3] J.M.D. Coey, Perspective and prospects for rare earth permanent magnets, Engineering 6 (2020) 118–130.
[4] L. Lou, Y. Li, X. Li, H. Li, W. Li, Y. Hua, W. Xia, Z. Zhao, H. Zhang, M. Yue, X. Zhang, Directional magnetization reversal enables ultrahigh energy density in gradient nanostructures, Adv. Mater. 33 (2021), e2102800.
[5] L. Zhao, J. He, W. Li, X. Liu, J. Zhang, L. Wen, Z. Zhang, J. Hu, J. Zhang, X. Liao, K. Xu, W. Fan, W. Song, H. Yu, X. Zhong, Z. Liu, X. Zhang, Understanding the role of element grain boundary diffusion mechanism in Nd-Fe-B magnets, Adv. Funct. Mater. 32 (2021), 2109529.
[6] E. Alonso, A.M. Sherman, T.J. Wallington, M.P. Everson, F.R. Field, R. Roth, R.E. Kirchain, Evaluating rare earth element availability: a case with revolutionary demand from clean technologies, Environ. Sci. Technol. 46 (2012) 3406–3414.
[7] T. Dutta, K.H. Kim, M. Uchimiya, E.E. Kwon, B.H. Jeon, A. Deep, S.T. Yun, Global demand for rare earth resources and strategies for green mining, Environ. Res. 150 (2016) 182–190.
[8] B. Zhou, Z. Li, C. Chen, Global potential of rare earth resources and rare earth demand from clean technologies, Minerals 7 (2017) 203-1–203-14.
[9] P. Falconnet, The economics of rare earths, J. Less Common. Met. 111 (1985) 9–15.
[10] Z. Chen, Global rare earth resources and scenarios of future rare earth industry, J. Rare Earths 29 (2011) 1–6.
[11] K. Binnemans, P.T. Jones, Rare earths and the balance problem, J. Sustain. Metall 1 (2015) 29–38.
[12] J.M.D. Coey, H. Sun, Improved magnetic properties by treatment of iron-based rare earth intermetallic compounds in anmonia, J. Magn. Magn Mater. 87 (1990) L251–L254.
[13] T. Iriyama, K. Kobayashi, N. Imaoka, T. Fukuda, H. Kato, Y. Nakagawa, Effect of nitrogen content on magnetic properties of $Sm_2Fe_{17}N_x$ (O<x<6), IEEE Trans. Magn. 28 (1992) 2326–2331.
[14] K. Kobayashi, R. Skomski, J.M.D. Coey, Dependence of coercivity on particle size in Sm2Fe17N3 powders, J. Alloys Compd. 222 (1995) 1–7.
[15] J.E. Shield, C.P. Li, D.J. Branagan, Microstructures and phase formation in rapidly solidified Sm–Fe and Sm–Fe–Ti–C alloys, J. Magn. Magn Mater. 188 (1998) 353–360.
[16] F.A.O. Cabral, S. Gama, E. de Morais, N.L. Sanjurjo, C.A. Rubeiro, C.C. Colucci, Study of thermal decomposition mechanism of the $Fe_{17}Sm_2N_3$ phase, IEEE Trans. Magn. 32 (1996) 4365–4367.
[17] T. Saito, Production of Sm-Fe-N bulk magnets by spark plasma sintering method, J. Magn. Magn Mater. 369 (2014) 184–188.
[18] S. Okada, K. Suzuki, E. Node, K. Takagi, K. Ozaki, Y. Enokido, Preparation of submicron-sized Sm2Fe17N3 fine powder with high coercivity by reduction-diffusion process, J. Alloys Compd. 695 (2017) 1617–1623.
[19] C. Lu, J. Zhu, J. Gong, X. Gao, A method to improving the coercivity of sintered anisotropic Sm-Fe-N magnets, J. Magn. Magn Mater. 461 (2018) 48–52.
[20] J.F. Herbst, J.J. Croat, Magnetization of RFe_3 intermetallic compounds: molecular field theory analysis, J. Appl. Phys. 53 (1982) 4304–4308.
[21] J.M. Yau, K.H. Cheng, C.H. Lin, T.S. Chin, Magnetic properties of $SmFe_3$ and its hydrogenation and nitrogenation, IEEE Trans. Magn. 29 (1993) 2851–2853.
[22] L. Schultz, K. Schnitzke, J. Wecker, M. Katter, High coercivities in Sm-Fe-Tm magnets, IEEE Trans. Magn. 26 (1990) 1373–1375.
[23] J. Wecker, M. Katter, K. Schnitzke, L. Schultz, Magnetic hardening of $(Sm,Zr)Fe_3$ alloys, J. Appl. Phys. 69 (1991) 5847–5849.
[24] T. Saito, T. Horita, D. Nishio-Hamane, Production of (Sm,Zr)Fe3 magnets and their magnetic properties, Mater. Sci. Eng. B 264 (2021) 114990-1–114990-4.
[25] M. Endoh, M. Iwata, M. Tokunaga, $Sm_2(Fe,M)_{17}N_x$ compounds and magnets, J. Appl. Phys. 70 (1991) 6030–6032.
[26] S. Sakurada, A. Tsutai, T. Hirai, Y. Yanagida, M. Sahashi, S. Abe, T. Kaneko, Structural and magnetic properties of rapidly quenched $(R,Zr)(Fe,Co)_{10}N_x$ (R=Nd,Sm), J. Appl. Phys. 79 (1996) 4611–4613.
[27] L. Peng, Q.H. Yang, H.W. Zhang, Y.Q. Song, J. Shen, Crystal structure and magnetic properties of hard magnetic Sm2Fe17N8 thin films with Co substitution, J. Magn. Magn Mater. 321 (2009) 442–445.
[28] M. Carbucicchio, M. Rateof, Ferromagnetic planar nanocomposites, Hyperfine Interact. 156/157 (2004) 581–593.